however, that the high accuracy of these determinations could not have been accomplished if the ligands present in the mixtures had not been pure and if their precise concentrations had not been known.

Conclusions

It has been shown that potentiometry may be applied successfully to the determination of protonation constants and stability constants when the experimental solutions consist of mixtures of ligands. It was found that all metal ions studied form normal 1:1 complexes with TMS and TDS. In addition mono, di-, and triprotonated metal complexes form with TDS, while only mono- and diprotonated metal complex species form with TMS. At slightly alkaline pH, the Fe^{3+} and Hg^{2+} chelates have a strong tendency toward hydroxo complex formation.

Acknowledgment. This work was supported by a research contract with Procter and Gamble Co., Cincinnati, OH.

Contribution from the Department of Chemistry and Quantum Institute, University of California, Santa Barbara, California 93106

Reaction Dynamics of Photosubstitution Intermediates of the Triruthenium Cluster $Ru_3(CO)_{12}$ As Studied by Flash Photolysis with Infrared Detection[1]

John A. DiBenedetto, David W. Ryba, and Peter C. Ford*

Received February 27, 1989

The reaction dynamics of intermediates formed by 308-nm XeCl excimer-laser excitation of the triruthenium cluster $Ru_3(CO)_{12}$ in room-temperature isooctane solution were studied by using a flash-photolysis apparatus with a tunable infrared laser probe source and Hg/Cd/Te fast-risetime IR detector. The primary photoreaction is the dissociation of CO to give $Ru_3(CO)_{11}$, which is rapidly trapped in second-order reactions by CO or by an added nucleophile such as tetrahydrofuran. The rate constants for such trapping are shown to be 2.4×10^9 and 6.1×10^9 M^{-1} s^{-1} for CO and THF, respectively. The intermediate $Ru_3(CO)_{11}(THF)$ reacts with CO to re-form $Ru_3(CO)_{12}$ via an apparent first-order dissociation of the THF with a rate constant about 2×10^6 s^{-1}. The flash-photolysis apparatus with the IR detection system is described in detail.

Introduction

Flash-photolysis techniques have proved especially valuable in probing the reaction dynamics of reactive organometallic intermediates of the type often proposed in thermal catalysis mechanisms but rarely directly observable in thermal reactions.[2] Optical (UV/visible spectral region) detection techniques, which have the advantage of good sensitivity and reliability, are the most commonly used with flash-photolysis experiments. In contrast, detection procedures using infrared frequencies have much greater diagnostic potential with regard to specific species or structural types being formed as transients.[3] This is especially true for metal carbonyl and other organometallic compounds, which often have sharp, characteristic transitions in vibrational spectra but rather broad and featureless absorptions in the electronic spectra. For this reason we have constructed a nanosecond flash-photolysis apparatus that uses an IR detection technique based on a lead salt diode laser as the probe source and a Hg/Cd/Te fast-risetime detector and have used this apparatus to study the photosubstitution mechanism of the triruthenium cluster $Ru_3(CO)_{12}$[4] in ambient-temperature solutions.

The photoreactions of $Ru_3(CO)_{12}$ in solution have been extensively investigated.[4-10] Early studies[5] reported the photofragmentation of the trinuclear cluster in the presence of various donor ligands; however, it was later demonstrated[8] that the photochemical pathways display a dependence on excitation wavelength now recognized to be common to di- and polynuclear metal carbonyls.[11] Photolysis at short wavelengths (<366 nm) leads predominantly to ligand substitution on the cluster (eq 1),

$$Ru_3(CO)_{12} + L \xrightarrow{h\nu} Ru_3(CO)_{11}L + CO \quad (1)$$

$$Ru_3(CO)_{12} + 3L \xrightarrow{h\nu} 3Ru(CO)_4L \quad (2)$$

while longer wavelength excitation (>400 nm) leads exclusively to fragmentation of the cluster framework (eq 2) under otherwise identical conditions. The photosubstitution pathway has previously been investigated by conventional flash-photolysis techniques at ambient temperature.[4] While this study, which used xenon lamp flash excitation and UV/vis detection methodology, provided kinetic information regarding transients as short-lived as 30 μs, it was clear that other key species with shorter lifetimes must also be involved. Subsequently, Wrighton and Bentsen[9] demonstrated the presence of possible such intermediates by using FTIR techniques to probe the spectra of low-temperature (90 K), glassy solutions of $Ru_3(CO)_{12}$ that had been subjected to photoexcitation at 313 nm. Described here are the reaction dynamics of such transients formed by laser flash photolysis of $Ru_3(CO)_{12}$ in ambient-temperature solutions as measured with a new apparatus using a XeCl excimer laser (308 nm) as the excitation source and the IR detection technique.

Experimental Section

Materials and Solutions. Triruthenium dodecacarbonyl was prepared as reported[12] and purified by sublimation in vacuo. Isooctane (Burdick and Jackson Spectrograde) was dried over CaH_2 and then distilled under N_2 immediately before use. Tetrahydrofuran (THF) was freshly distilled under N_2 from a sodium benzophenone ketyl solution.

Solutions for photolysis studies were prepared under N_2 with freshly distilled isooctane by using Schlenk techniques. Concentrations for transient bleaching experiments were chosen to give infrared absorbances 0.2–0.5 at the absorbance bands used as monitoring frequencies for a

(1) Reported in part at the 1987 Pacific Conference on Chemistry and Spectroscopy, Irvine, CA, October 1987, and at the 196th National Meeting of the American Chemical Society, Los Angeles, September 1988 (INOR 382).
(2) Wink, D. A.; Ford, P. C. *J. Am. Chem. Soc.* **1986**, *108*, 4838–4842; **1987**, *109*, 436–442.
(3) (a) Hermann, H.; Grevels, F.-W.; Henne, A.; Schaffner, K. *J. Phys. Chem.* **1982**, *86*, 5151–5154. (b) Ouderkirk, A. J.; Wermer, P.; Schultz, N. L.; Weitz, E. *J. Am. Chem. Soc.* **1983**, *105*, 3354–3355. (c) Moore, B. D.; Simpson, M. B.; Poliakoff, M.; Turner, J. J. *J. Chem. Soc., Chem. Commun.* **1984**, 972. (d) Poliakoff, M.; Weitz, E. *Adv. Organomet. Chem.* **1986**, *25*, 277–316. (e) Dixon, A. J.; Healy, M. A.; Hodges, P. M.; Moore, B. D.; Poliakoff, M.; Simpson, M. B.; Turner, J. J.; West, M. A. *J. Chem. Soc., Faraday Trans. 2* **1986**, *82*, 2083–2092. (f) Wasserman, E. P.; Bergman, R. G.; Moore, C. B. *J. Am. Chem. Soc.* **1988**, *110*, 6076–6084.
(4) Desrosiers, M. F.; Wink, D. A.; Trautman, R.; Friedman, A. E.; Ford, P. C. *J. Am. Chem. Soc.* **1986**, *108*, 1917–1927.
(5) Johnson, B. F. G.; Lewis, J.; Twigg, M. V. *J. Organomet. Chem.* **1974**, *67*, C75–76.
(6) Desrosiers, M. F.; Ford, P. C. *Organometallics* **1982**, *1*, 1715–1716.
(7) Mailito, J.; Markiewicz, S.; Poë, A. *Inorg. Chem.* **1982**, *21*, 4335–4338.
(8) Desrosiers, M. F.; Wink, D. A. *Inorg. Chem.* **1985**, *24*, 1–2.
(9) Bentsen, J. G.; Wrighton, M. S. *J. Am. Chem. Soc.* **1987**, *109*, 4530–4544.
(10) Burke, M. R.; Takats, J.; Grevels, F.-W.; Reuvers, J. G. A. *J. Am. Chem. Soc.* **1983**, *105*, 4092–4093.
(11) Poë, A. J.; Sekhar, C. V. *J. Am. Chem. Soc.* **1986**, *108*, 3673–3679.
(12) Eady, C. R.; Jackson, P. F.; Johnson, B. F. G.; Lewis, J.; Malatesta, M. C.; McPartlin, M.; Nelson, W. J. H. *J. Chem. Soc., Dalton Trans.* **1980**, 383–392.

0020-1669/89/1328-3503$01.50/0

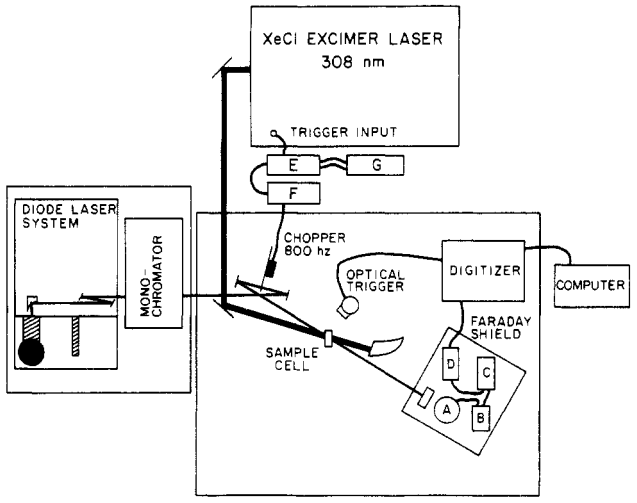

Figure 1. Block diagram for flash-photolysis apparatus with IR detection system. Labelled components are as follows: A, Hg/Cd/Te detector; B, preamplifier; C, amplifier; D, line driver (used only in some applications); E, sync box; F, chopper controller; G, BNC delay generator.

solution in the short path length (0.5 or 1.0 mm) photolysis cell. At these concentrations the corresponding absorbance of the solution at the 308-nm excitation wavelength was about 0.2. Once prepared as described, the solutions were bubbled with the desired gas mixture and appropriate concentrations of other reagents added with a microliter syringe under N_2.

Procedures for Handling Photolysis Solutions. Solutions were passed through the photolysis cell by using a simple flow apparatus consisting of a Schlenk tube reservoir, large syringe, photolysis cell, and connecting stainless-steel transfer tubes. This provided a gastight system for continuous delivery of the solution through the photolysis cell at a rate where each laser pulse irradiated a fresh solution. The photolysis cell consisted of a modified McCarthy IR cell with CaF_2 windows, a 0.5–1.0-mm Teflon spacer, and Luer-lock type connectors to the stainless-steel tubing of the flow apparatus. Photolysis solutions were loaded into the drive syringe from the Schlenk tube under a positive pressure of the appropriate gas and then delivered to the photolysis cell under manual pressure with a flow rate of several milliliters per minute during a 50 or 200 laser shot data acquisition. Electronic spectra of the photolysis solutions were recorded before and after each experimental sequence to ensure that net photolysis had not significantly modified the solution characteristics.

Flash-Photolysis Apparatus with IR Detection. This apparatus used in these studies is described in Figure 1. The excitation source was either a Lambda Physik EMG 201 MSC XeCl excimer laser or a Lambda Physik LPX 105 XeCl excimer laser operating at 308 nm, the output of which was directed through the CaF_2-windowed IR flow cell described above. The detection system is designed to observe temporal transmittance changes in the IR spectral region. A Spectra Physics/Laser Analytics Model SP5800 laser source assembly was used as the IR probe source. The laser head was a model SP5731 closed-cycle He refrigerator, and this was mounted on a table separate from that on which were mounted the photolysis sample cell and the IR detector assembly in order to prevent transmission of the low-frequency noise associated with the refrigerator motor. (Acoustical tile was placed beneath each table leg and under the Newport Research breadboard optical table top to damp vibrations.) The laser head included four interchangeable lead salt diode lasers, each tunable over roughly a 100-cm^{-1} range (depending on the individual lasers) by use of the Model SP5820 current controller and SP 5720 temperature controller. The frequency ranges of the four diodes used were centered at 1933, 2095, 1795, and 1705 cm^{-1}. The laser operation was often multimode, especially at high current operation. For this reason, the roughly 2–3-mm-diameter IR beam from the laser was passed through a CVI Digikrom 240 monochromator to determine the exact frequency and to ensure single laser line transmission. The probe beam (about 2–3-mm diameter) was then passed through the center of the region in the sample cell excited by the pump beam (about 6–7-mm diameter), which entered the sample cell at an angle about 30° from that of the probe. The probe beam then passed through the blades of a Stanford Research Systems Model 540 chopper (operating at 800 Hz) to produce a 145-μs-wide square wave, to which was synchronized the excimer-laser pulse (see below). The chopped probe was then refocused by a 1-in.-diameter ZnSe (F-3) lens situated about 5 cm from the Santa Barbara Research Center PV Hg/Cd/Te fast-risetime detector to provide a more homogeneous output at the 1-mm^2 detector plane.

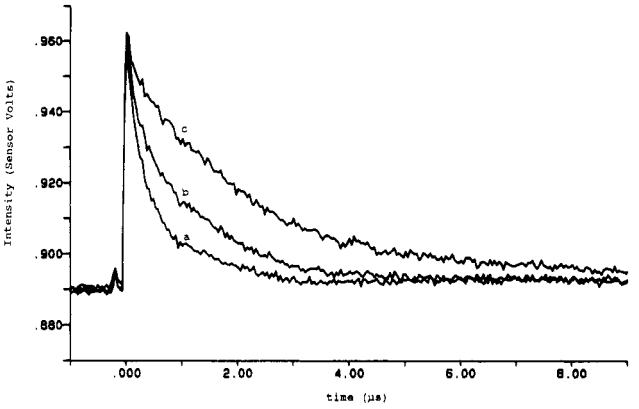

Figure 2. Temporal IR intensities at 2061 cm^{-1} following laser excitation of a solution of $Ru_3(CO)_{12}$ (100 μM) in isooctane solution under a 10% CO/90% Ar mixture (1 atm). Curves a–c were recorded for solutions containing THF in the respective concentrations 1.2×10^{-4}, 4.8×10^{-4}, and 12×10^{-4} M. These curves are the signal average of 200 laser shots each but are raw data taken from the digital oscilloscope before base-line subtraction or smoothing procedures were used.

The excimer laser was synchronized to the chopper output by counting down the photodiode output of the SRS chopper sync (800 Hz) to isolate a specific blade (to reduce time jitter) and lower the repetition rate to 2" (4 Hz in the present case). A BNC Model 7065 delay generator was used to fine-tune the excimer/chopper time overlap. A 15-V output from the syncbox is used to fire the laser while a Xenon Corp. photodetector is used to trigger the digital oscilloscope from laser light scattered from an optical element. Digital posttriggering allowed the capture of the entire 145-μs square-wave signal at 125-MHz resolution regardless of the trigger position on the square wave. While the counter is allowed for a small jitter of the laser firing time during the square-wave transmittance (1 μs owing to chopper position uncertainty), optical triggering of the LeCroy 9400 scope synchronized the laser flash event to the recorder with better than 10-ns resolution. The low jitter allowed signal averaging with no appreciable loss to the single-shot time resolution.

The photocurrent output from the IR detector was amplified by a low-noise Perry Model 490 fast-risetime preamplifier and a 10× voltage-following amplifier then terminated into a 50-Ω input of a LeCroy 9400 digital oscilloscope through an 18 inch double shielded 50-Ω cable. The system response time was determined to be <80 ns. (The detector, preamplifier, amplifier and 12-V battery power supply were enclosed in a $^1/_8$ in. thick aluminum Faraday cage electrically isolated from the optical table.) The amplitude versus time plots of IR intensity of each laser shot were recorded by the oscilloscope, which averages 50 shots of 8-bit resolution to give a 16-bit resolution trace. The 16-bit signal-averaged data were transferred to an IBM AT computer using LeCroy Catalyst software via a National Instruments PC-3 GPIB interface. This allows the capture of ≥10-mV transients on a 1800-mV signal with 60-μV sensitivity. ASYSTANT programming (McMillan software) was used to subtract an averaged base-line shot (laser blocked at the sample) from the data accumulated during excitation (Figure 2). The temporal absorbances were then calculated by using the change in transmitted intensity (eq 3) plus the total transmitted light determined with and without

$$\mathrm{Abs}(t) = -\log [(\Delta I + I)/I_0] \qquad (3)$$

sample absorption (I and I_0, respectively). The Abs(t) data were then numerically fitted to kinetics equations after smoothing with a low pass filter (Blackman window) and data reduction.

In the present study the pump laser was attenuated by using fine-mesh screens or quartz plates to reduce the laser power. Excitation was carried out 4 Hz at an average laser pulse intensity of 24 mJ/cm^2 over a typical irradiation area of 0.25 cm^2. Given the typically 1.0-mm path length of the photolysis cell, the excitation volume was about 25 μL. At higher laser pulse energies, shock waves generated in the sample cell could be observed with the IR detector even when the cell was filled with pure solvent. However, shock type phenomena were minimized at the pump laser conditions described here. Another major source of noise was reproducible EMI from the laser thyratron tube firing, which was substantially reduced by installing a line filter and by shielding the 220-V power line of the LP EMG 201 MSC excimer laser. Base-line subtraction techniques were also successful in numerically eliminating most of the laser EMI noise as well as signal "droop" due to the capacitively coupled input of the fast risetime current preamplifier. The EMI noise was significantly less with the newer model LPX 105 laser. In addition, reducing the incident intensity of the IR probe source and reducing the

incident intensity of the UV pump source decreased signal droop and shock type noise, respectively, to give uncorrected IR signal vs time plots of the quality shown in Figure 2.

Results and Discussion

As noted above, earlier studies[4,8] have shown that short wavelength excitation of $Ru_3(CO)_{12}$ in solution leads predominantly to photolabilization of CO resulting in net photosubstitution when other ligands are present (eq 1). In tetrahydrofuran solution, conventional microsecond flash-lamp photolysis techniques were able to observe a solvated intermediate believed to be $Ru_3(CO)_{11}THF$. This re-formed $Ru_3(CO)_{12}$ by thermal back-reaction with CO (eq 4, S = THF). Although ligand photosubstitutions

$$Ru_3(CO)_{11}S + CO \rightarrow Ru_3(CO)_{12} + S \qquad (4)$$

were also seen in saturated hydrocarbon solvents, no intermediates were seen in the earlier flash-photolysis studies, apparently because the reactions equivalent to eq 4 were too rapid. Evidence of solvated hydrocarbon complexes as well as of the dissociated species $Ru_3(CO)_{11}$ were reported by Bentsen and Wrighton,[9] who used a low-temperature IR cell to record the spectra of intermediates from the photolysis of $Ru_3(CO)_{12}$ in glassy hydrocarbon solvents at 90 K. The present studies employed nanosecond flash photolysis with IR detection techniques to probe the reaction dynamics of this system in ambient-temperature fluid solutions.

The IR spectrum of $Ru_3(CO)_{12}$ in isooctane displays four bands in the ν_{CO} region at 2061 vs, 2031 s, 2017 m, and 2011 m cm^{-1}. When a solution of $Ru_3(CO)_{12}$ (typically $1-2 \times 10^{-4}$ mol L^{-1}) in this solvent under argon was subjected to excimer-laser excitation at 308 nm, transient bleaching was observed at the IR monitoring frequency of 2061 cm^{-1}, indicating the disappearance of $Ru_3(CO)_{12}$. Given the reported extinction coefficient of $Ru_3(CO)_{12}$ at this frequency (2.45×10^4 M^{-1} cm^{-1}),[9] the initial transmittance change corresponds to a lower limit of 12% bleaching of the parent compound. Only a lower limit can be calculated owing to the unknown extinction coefficient of the transient, which also absorbs at this frequency; other bands of $Ru_3(CO)_{12}$ suffer similar complications. The bleaching was followed by decay back to the starting transmittance. Numerical conversion of transmittance to absorbance gave a decay curve that could be fit to the equation for second-order kinetics ($Abs(t) = B + (Ct + A)^{-1}$). Unfortunately, $\Delta\epsilon$ is unknown, but a rough estimate (7×10^3 M^{-1} cm^{-1} at 2061 cm^{-1}) allows estimation of concentration changes and of the second-order rate constant, 5×10^9 M^{-1} s^{-1}. IR transmittance changes monitored at the strong ν_{CO} band 2031 cm^{-1} also gave second-order kinetic behavior.

Temporal spectral changes over the frequency range 2020–2070 cm^{-1} were recorded for samples of $Ru_3(CO)_{12}$ in isooctane under argon by tuning the probe laser beam in 2-cm^{-1} increments through this region (Figure 3). In this figure, negative absorbances indicate bleaching of the bands at 2031 and 2061 cm^{-1} characteristic of the starting complex; positive absorbances indicate ν_{CO} bands of new species formed by the flash. Notably, the positive absorbance at 2036 cm^{-1} is consistent with the report from the low-temperature study of a strong band at 2033 cm^{-1} present in the IR spectrum of the two different isomeric forms of $Ru_3(CO)_{11}$, the product of CO photodissociation from $Ru_3(CO)_{12}$. However, the "terminal form" isomer (I, where all CO's are bound to single Ru's) has been reported to have a strong band at 2054 cm^{-1} as well; thus, we conclude that the likely isomer is the "bridged form" II, which has been proposed to include one bridging CO. A more convincing confirmation of this conclusion would be observation of the bridging ν_{CO} IR band at 1836 cm^{-1} reported for II.[9] However, at 90 K this band is a factor of 13 less intense than that at 2033 cm^{-1}, and the results of attempts to demonstrate its presence for the room-temperature transient were equivocal. According to a previous report, the terminal form, the initial product of CO photodissociation from $Ru_3(CO)_{12}$, rearranges to the more stable bridging form even at 90 K. In the present case, we conclude that this rearrangement appears to occur within 80 ns, the observed detector/preamplifier response time. All absorption and bleaching features of Figure 4 decayed to base line by second-order kinetics on the same time scale, an observation

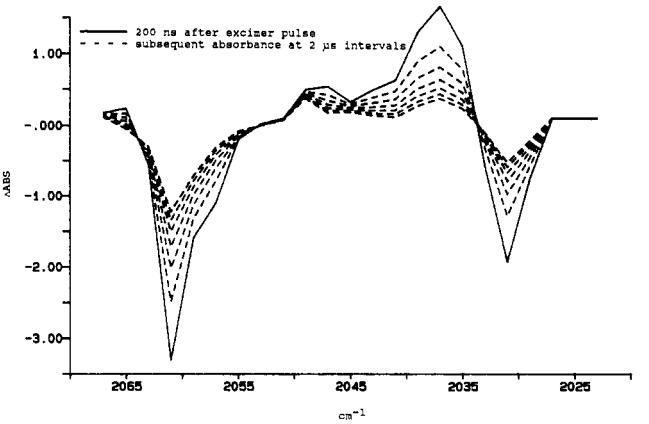

Figure 3. IR difference spectrum of the transient formed by 308-nm flash photolysis of $Ru_3(CO)_{12}$ (100 μM) in ambient-temperature isooctane solution under Ar. The solid curve was recorded 200 ns after the flash. Subsequent curves were recorded at regular intervals of 2.0 μs. Negative peaks are due to bleaching of bands of the starting material; positive bands represent absorptions belonging to flash-generated transients.

which suggests that the spectral features indicate a single reactive intermediate or a collection of species in equilibrium interconverting rapidly relative to trapping with CO. These data are consistent with the operation of eq 5 and 6.

$$Ru_3(CO)_{12} \xrightarrow{h\nu} Ru_3(CO)_{11} + CO \qquad (5)$$

$$Ru_3(CO)_{11} + CO \xrightarrow{k_{CO}} Ru_3(CO)_{12} \qquad (6)$$

When the 308-nm excimer flash photolysis of $Ru_3(CO)_{12}$ in isooctane was carried out in the presence of added CO, the observed relaxation of the transient to the starting material was much faster and was exponential. The rate constants (k_{obs}) obtained by fitting these curves to a first-order kinetics equation ($Abs(t) = A - Be^{-Ct}$) (Figure 4) proved to be dependent on the CO concentration. The values $(2.3 \pm 0.3) \times 10^5$ s^{-1} under a 1/99 CO/Ar mixture (1 atm), $(1.3 \pm 0.4) \times 10^6$ s^{-1} under 5/95 CO/N_2 and $(2.2 \pm 0.4) \times 10^6$ s^{-1} under 10/90 CO/Ar mixture were determined. The reported solubility of CO in octane is 0.012 mol/atm and in cyclohexane is 0.0092 mol/atm,[4] so 0.010 mol/atm would be a reasonable estimate for CO solubility in isooctane. Thus, the above k_{obs} values divided by the estimated [CO] under the various pressures give a value of $(2.4 \pm 0.4) \times 10^9$ M^{-1} s^{-1} for k_{CO} under these conditions. This value is somewhat smaller than that estimated above from photolysis under second-order conditions. However, we consider the value determined under first-order conditions to be the more reliable owing to its independence of estimates of $\Delta\epsilon$ at the exact operating frequency of the laser.

In tetrahydrofuran solution, 308-nm excimer flash photolysis led to the formation of transients with much longer lifetimes than those seen in isooctane. Indeed, the transient proved to be sufficiently long-lived that the decay continued over many of the 145-μs square waves generated by the 800-Hz chopper.[13] This long-lived transient can be attributed to the trapping of the $Ru_3(CO)_{11}$ by the donor solvent to give the more stable intermediate $Ru_3(CO)_{11}THF$. Similar conclusions have been drawn from conventional flash-photolysis studies of $Ru_3(CO)_{12}$ in THF[4] and from IR studies of the products of $Ru_3(CO)_{12}$ photolysis in 90 K 2-MeTHF glasses.[9]

When the flash photolysis was carried out in isooctane with added THF (10^{-4}–0.09 M), the lifetimes of the transients observed were much longer than in isooctane alone, and the rates of decay back to $Ru_3(CO)_{12}$ were functions both of [CO] and of [THF]. Temporal spectral changes showed not only bleaching of the bands

(13) For long-lived transients (decays as long as seconds) the changes in the IR intensities at the monitoring frequency could be followed by sampling the maximum of the square wave probe beam signal over a period of time.

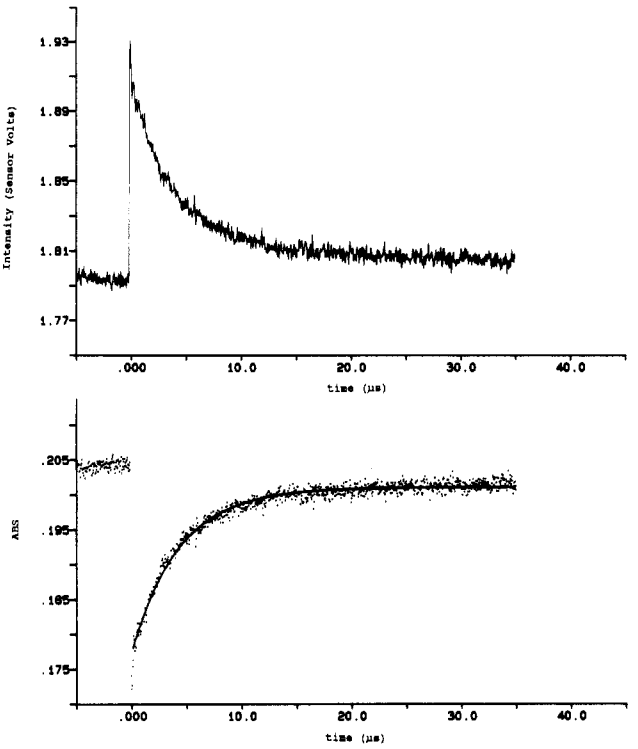

Figure 4. Top: Temporal changes in IR transmittance of a solution of $Ru_3(CO)_{12}$ (in isooctane under 1% CO in argon) monitored at 2061 cm^{-1} (average of 200 laser shots). Bottom: Data in the upper part converted to absorbance and fitted according to the equation $f(t) = A - B[e^{-Ct}]$ with $A = 0.201$, $B = 0.0237$, and $C = 0.232 \times 10^6$ s^{-1}.

characteristic of $Ru_3(CO)_{12}$ but also transient absorption at 2049 cm^{-1}, the absorption frequency reported[9] for the substituted cluster $Ru_3(CO)_{11}$(2-MeTHF) at low temperature. Decay rates measured by following the transient absorption at 2049 cm^{-1} proved to be identical, within experimental uncertainty, with those measured by following regeneration of $Ru_3(CO)_{12}$ at 2061 cm^{-1} under the same conditions.

The mechanism shown in Scheme I has been postulated[4,9] for the photolabilization reactions of $Ru_3(CO)_{12}$ in the presence of a weakly coordinating donor such as THF. If the reaction were

Scheme I

$$Ru_3(CO)_{12} \xrightarrow{h\nu} Ru_3(CO)_{11} + CO$$

$$Ru_3(CO)_{11} + S \underset{k_{-S}}{\overset{k_S}{\rightleftharpoons}} Ru_3(CO)_{11}S$$

$$Ru_3(CO)_{11} + CO \xrightarrow{k_{CO}} Ru_3(CO)_{12}$$

run in a hypothetically noncoordinating medium in which both S and CO were variables, the kinetics of transient decay would be described by

$$-\frac{d[Ru_3(CO)_{11}S]}{dt} = \frac{d[Ru_3(CO)_{12}]}{dt} = k_{obs}[Ru_3(CO)_{11}S] \quad (7)$$

where

$$k_{obs} = k_{CO}[CO]\frac{k_{-S}}{k_S[S] + k_{CO}[CO]} \quad (8)$$

The reciprocal of this relationship is

$$k_{obs}^{-1} = \frac{k_S[S]}{k_{CO}k_{-S}}[CO]^{-1} + k_{-S}^{-1} \quad (9)$$

Thus, a plot k_{obs}^{-1} vs [S] should be linear with the slopes equal $k_S/k_{-S}k_{CO}[CO]$ and the intercepts equal k_{-S}^{-1}.

In this context, the dynamics of $Ru_3(CO)_{12}$ re-formation after the flash photolysis in isooctane solution were examined as functions of the CO pressure and of the concentrations of added

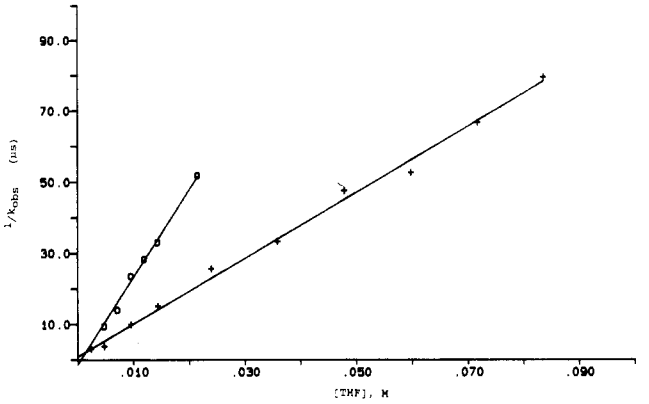

Figure 5. Plots of k_{obs}^{-1} vs [THF] for the recovery of $Ru_3(CO)_{12}$ as monitored at 2061 cm^{-1} subsequent to 308-nm flash photolysis in isooctane solution under 10/90 CO/N_2 (crosses) or 5/95 CO/N_2 (circles) with various concentrations of added THF in isooctane solution.

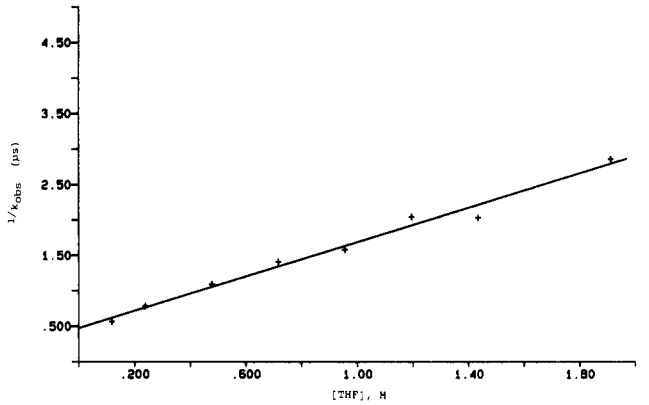

Figure 6. Plot similar to Figure 5 but with data collected for the flash photolysis of $Ru_3(CO)_{12}$ under 10% CO in isooctane containing THF in the lower concentration range (0.1–1.9) $\times 10^{-3}$ M.

THF (e.g., see Figure 2). The relaxation kinetics of solutions equilibrated under a 10/90 CO/N_2 gas mixture (1.0 atm) displayed first-order kinetics consistent with eq 7. The k_{obs} values determined from these data proved to be strongly dependent on the concentration of THF. A plot of k_{obs}^{-1} vs [THF] is linear over the range 0.003–0.08 M (Figure 5) with the slope (0.92 ± 0.1) $\times 10^{-3}$ M^{-1} s. An intercept near zero on this scale was the case, but the scatter leaves this value (0.2 ± 1.5 μs) highly uncertain. A second, independent, run carried out by using a series of smaller THF concentrations ((0.1–1.9) $\times 10^{-3}$ M) with the 10% CO mixture gave a similar linear plot of k_{obs}^{-1} vs [THF] (Figure 6) with a slope of (1.21 ± 0.1) $\times 10^{-3}$ M^{-1} s^{-1} and a clearly nonzero intercept of (0.48 ± 0.05) $\times 10^{-6}$ s. Under 5% CO mixture, a linear plot was observed for the k_{obs} data from a similar run over the [THF] range 0.004–0.02 M (Figure 5), the slope being (2.46 ± 0.2) $\times 10^{-3}$ M^{-1} s. The differences in the slopes are consistent with the inverse [CO] dependence predicted by eq 9.

According to eq 9 the intercept of the k_{obs}^{-1} vs [THF] plot of Figure 6 should equal k_{-S}^{-1}. From this, the value $k_{-S} = (2.1 \pm 0.2) \times 10^6$ s^{-1} can be calculated. Equation 9 also suggests the relationship slope = $k_S/k_{CO}k_{-S}$[CO]. Thus, values of the slope from Figure 6 (1.2 ± 0.1 $\times 10^{-3}$ M^{-1} s), k_{CO} (2.4 ± 0.4 $\times 10^9$ M^{-1} s^{-1}; see above), and the concentration of CO in equilibration with a partial pressure of 0.1 atm ($[CO]_{est} = 1 \times 10^{-3}$ M) give the calculated k_S/k_{-S} ratio: 2.9 ± 0.6 $\times 10^3$ M^{-1}. This would be the equilibrium constant for the trapping of $Ru_3(CO)_{11}$ by THF in the isooctane solvent. From the value for k_{-S} calculated by the intercept in Figure 6, k_S, the rate constant for trapping $Ru_3(CO)_{11}$ by THF can be calculated to equal 6.1 ± 1.2 $\times 10^9$ M^{-1} s^{-1}, roughly twice as large as k_{CO}. These latter values are subject to significant uncertainty owing to the multiplied errors in slopes and intercepts; however, it does appear that, under these conditions, THF can trap the unsaturated $Ru_3(CO)_{11}$ cluster with a rate constant somewhat greater than that for trapping by CO.

The rate constants for trapping of the $Ru_3(CO)_{11}$ intermediate by CO or THF are each close to that calculated for a diffusion-limited reaction in the isooctane solvent.[14] Thus, this unsaturated cluster must be but weakly solvated by the isooctane. In contrast, but not surprising, the reactivity of the "THF solvate" is orders of magnitude less. Comparable high reactivity has been reported for the mononuclear unsaturated intermediate $(\eta^5\text{-}C_5H_5)Co(CO)$ formed by CO photodissociation from the dicarbonyl in cyclohexane, which reacts with various two-electron donors with second-order rate constants $>10^9$ M^{-1} s^{-1}.[3f] However, hydrocarbons appear to stabilize the $Cr(CO)_5$ intermediate (formed from $Cr(CO)_6$) more strongly; in cyclohexane this species reacts with CO with a rate constant (3×10^6 M^{-1} s^{-1}) about 3 orders of magnitude faster than in more weakly binding fluorocarbon solvents.[15] Among the few examples of dinuclear intermediates which have been analogously studied, both $Mn_2(CO)_9$[16] and $[(\eta^5\text{-}C_5H_5)Fe_2(\mu\text{-}CO)_3]$[17] (prepared, respectively, by CO photodissociation from $Mn_2(CO)_{10}$ and $[(\eta^5\text{-}C_5H_5)_2Fe_2(CO)_4]$) react with two-electron donors in cyclohexane solutions relatively slowly, i.e., with second-order rate constants near 10^6 M^{-1} s^{-1}. These intermediates each displayed IR spectra consistent with the unsaturation resulting from CO photodissociation being in part compensated by movement of one terminal carbonyl to a bridging or semibridging position. Similar rearrangement is available to $Ru_3(CO)_{11}$ and indeed has been proposed above to be the case. Thus, the surprising observation that this intermediate is so reactive with two-electron donors in alkane solutions suggests that any stabilization from such carbonyl bridging in the triruthenium cluster has but a minor effect on the dynamics of the bimolecular reactivity.

In summary, the mechanism described by Scheme I appears to be valid for S = THF and the medium being isooctane solution. The $Ru_3(CO)_{11}$ species must be but weakly solvated by the isooctane given that the rate constants k_{CO} and k_S have the values $2.4 \pm 0.4 \times 10^9$ M^{-1} s^{-1} and $6.1 \pm 1.2 \times 10^9$ M^{-1} s^{-1}, respectively, values which are less than 1 order of magnitude smaller than the calculated diffusion limit in this medium.

Acknowledgment. This research was sponsored by a grant (DE-FG03-85ER13317) from the Division of Chemical Sciences, Office of Basic Energy Science, U.S. Department of Energy, and by grants (CHE84-19283 and CHE87-22561) from the National Science Foundation. The instrumentation components used to construct the apparatus described were funded as follows: LP EMG 201 excimer laser, NSF grant for chemical instrumentation (CHE84-1302); LP LPX 105 excimer laser, NSF Grant CHE87-22561; Spectra Physics-Laser Analytics IR laser, UCSB Faculty Research Committee Research Opportunity Grant and NSF Grant CHE84-1928; optical hardware, detection electronics, and computers, Amoco Technology Co. and the UCSB Quantum Institute. We thank Dr. T. L. Netzel of the Amoco Technology Co. for his advice and encouragement and Dave Wall of Spectra Physics/Laser Analytics for advice in applications of the IR laser system.

(14) (a) The diffusion rate limit in isooctane was calculated by using Fick's 1st law and the viscosity of isooctane (0.504 cp at 20 °C) to be 1.3×10^{10} M^{-1} s^{-1}.[15b] (b) Murov, S. L. *Handbook of PhotoChemistry*; Marcel Dekker, Inc.: New York, 1973; p 86.
(15) (a) Bonneau, R.; Kelly, J. M. *J. Am. Chem. Soc.* **1980**, *102*, 1220–1221. (b) Yang, G. K.; Vaida, V.; Peters, K. S. *Polyhedron* **1988**, *7*, 1619–622.
(16) Church, S. P.; Hermann, H.; Grevels, F.-W.; Schaffner, K. *J. Chem. Soc., Chem. Commun.* **1984**, 785–786.
(17) Dixon, A. J.; Healy, M. A.; Poliakoff, M.; Turner, J. J. *J. Chem. Soc., Chem. Commun.* **1986**, 994–996.

Contribution from the Department of Chemistry,
The University of Texas at Austin, Austin, Texas 78712

Reductive Quenching of Ruthenium Polypyridyl Sensitizers by Cyanometalate Complexes

Thomas E. Mallouk,* Jonathan S. Krueger, James E. Mayer, and Christopher M. G. Dymond

Received December 6, 1988

Laser flash photolysis/transient absorbance and emission spectroscopy were used to probe the nature of the reductive quenching of ruthenium polypyridyl sensitizers by cyanometalate electron donors in aqueous solution. Quenching rate constants and approximate cage escape efficiencies were measured for a number of donor/sensitizer pairs; octacyanometalates ($Mo(CN)_8^{4-}$, $W(CN)_8^{4-}$) exhibit much higher cage escape efficiencies, typically 40–80%, than do hexacyanometalates ($Fe(CN)_6^{4-}$, $Os(CN)_6^{4-}$). Cage escape efficiencies vary with the overall charge of the sensitizer; geminate ion pair recombination competes most efficiently with cage escape when the electron donor and acceptor have 4+ and 4− overall charges, respectively. No dependence of cage escape efficiency on thermodynamic driving force for the back-electron-transfer reaction is observed. Little or no dependence on ionic strength or counterion is observed. Steady-state and time-resolved luminescence experiments with $Ru(bpy)_3^{2+}$ (bpy = 2,2′-bipyridine) show that the quenching process is dynamic at low cyanometalate concentrations and that association of the cationic sensitizer with the anionic cyanometalates occurs at higher concentrations. Even under these conditions, quantum yields for charge separation approach unity with octacyanometalate electron donors.

Since Adamson and Gafney first proposed electron-transfer quenching experiments involving tris(2,2′-bipyridine)ruthenium(II) in 1972, this molecule has been widely studied by photochemists.[1] Its strong electronic transitions in the visible and near-ultraviolet regions of the spectrum, strong luminescence in solution, relatively long metal to ligand charge-transfer (MLCT) state lifetime (670 ns),[2] and disinclination to undergo unimolecular photoreactions make it a superior photosensitizer.[3]

Since the first oxidation potential of $Ru(bpy)_3^{2+}$ is +1.29 V vs SCE (saturated calomel electrode) in acetonitrile[4a] and the excess free energy of the excited state over that of the ground state is 2.10 eV, it is apparent that the excited-state species $*Ru(bpy)_3^{2+}$ must be a strong reducing agent. Accordingly, many electron-transfer studies involving $Ru(bpy)_3^{2+}$ have entailed oxidative quenching of the excited state:[1,5-7]

$$Ru(bpy)_3^{2+} \xrightarrow{h\nu} *Ru(bpy)_3^{2+} \quad (1)$$

$$*Ru(bpy)_3^{2+} + Q \rightarrow Ru(bpy)_3^{3+} + Q^- \quad (2)$$

In an analogous manner, the first reduction potential for $Ru(bpy)_3^{2+}$, −1.33 V vs SCE in acetonitrile,[4a] indicates that *Ru-

* To whom correspondence should be addressed.

(1) Gafney, H. D.; Adamson, A. W. *J. Am. Chem. Soc.* **1972**, *94*, 8238.
(2) Bensasson, R.; Salet, C.; Balzani, V. *J. Am. Chem. Soc.* **1976**, *98*, 3722.
(3) Whitten, D. G. *Acc. Chem. Res.* **1980**, *13*, 83.
(4) (a) Creutz, C.; Sutin, N. *Inorg. Chem.* **1976**, *15*, 496. (b) Toma, H. E.; Creutz, C. *Inorg. Chem.* **1977**, *16*, 545.
(5) Navon, G.; Sutin, N. *Inorg. Chem.* **1974**, *13*, 2159.
(6) Bock, C. R.; Meyer, T. J.; Whitten, D. G. *J. Am. Chem. Soc.* **1974**, *96*, 4710.
(7) Bock, C. R.; Meyer, T. J.; Whitten, D. G. *J. Am. Chem. Soc.* **1975**, *97*, 2909.

0020-1669/89/1328-3507$01.50/0